Marine Geodesy, 31: 281–298, 2008

ISSN: 0149-0419 print / 1521-060X online
DOI: 10.1080/01490410802466652

Taylor & Francis
Taylor & Francis Group

Automated Derivation of Bathymetric Information from Multi-Spectral Satellite Imagery Using a Non-Linear Inversion Model

HAIBIN SU, HONGXING LIU, AND WILLIAM D. HEYMAN

Department of Geography, Texas A&M University, College Station, Texas, USA

Most previous studies utilized a log-linear regression model to invert multi-spectral images into bathymetric data. Based on the Levenberg-Marquardt optimization algorithm, we developed an automated method for calibrating the parameters for a non-linear inversion model. Our method has been successfully applied to an IKONOS multispectral image. We compared depth data derived from our model to those estimated using a conventional log-linear inversion model. Bathymetric data derived from the non-linear inversion model are slightly more accurate and stable, particularly for deeper benthic habitats, than those derived from a conventional log-linear model although their overall performances are very similar.

Keywords Water depth, inversion, IKONOS, optimization, Levenberg-Marquardt method

Introduction

Bathymetric information is of fundamental importance to coastal and marine planning and management, nautical navigation, and scientific studies of marine environments. Monitoring navigation channels for shipping traffic safety and mapping underwater sand bars, rocks, shoals, reefs and other hazardous marine features relies on accurate and up-to-date water depth measurements (Jupp 1989). Some nearshore activities (recreation, fishing, and aquaculture) and offshore engineering works such as cable and pipeline laying, dredging, oil drilling, and beach nourishment, also require knowledge of bathymetry. Bathymetric data are essential for modeling and predicting coastal storm surge and flooding, oceanic circulation, and tsunami propagation. Scientists have employed bathymetric data to identify and map submerged reefs and other morphological features on the seafloor (Jupp et al. 1985; Storlazzi et al. 2003; Brock et al. 2004; Finkl et al. 2005a, 2005b). In addition, water depth information has been used to perform water-column corrections of remotely sensed images in order to improve the accuracy of benthic habitat maps (Mumby et al. 1998; Conger et al. 2006; Mishra et al. 2006). Global bathymetric data at a spatial resolution of 2 minutes (4 km at the equator) have been derived for all of the world's oceans based on marine gravity field measurements from the Geosat and ERS-1 satellite radar altimeters (Smith and Sandwell 1997). This coarse resolution bathymetric data set offers a complete view of the global seafloor topography. It is particularly valuable for studying seamounts, oceanic plateaus,

Received 11 May 2008; accepted 4 September 2008.
Address correspondence to Haibin Su, Department of Geography, Texas A&M University, College Station, TX77843. E-mail: suhaibin@geog.tamu.edu

and other large underwater geologic structures (Smith and Sandwell 1997). Nevertheless, it is not adequate for many coastal applications that require detailed bathymetry information. Despite the great demand for accurate, high-resolution seafloor topography data, present availability of such data remains incomplete and spatially limited.

Traditional bathymetric charts are based on individual soundings accumulated during decades of ship-borne surveying operations. Ship-borne surveys with single- or multi-beam echo sounders can operate to depths in excess of 500 m by sensing and tracking acoustic pulses. Singe-beam sonar (Sound Navigation and Ranging) systems have been used since the 1950s by survey vessels to measure water depths along transect lines, but these lines are generally sparsely distributed. Since the 1980s, more accurate multi-beam echo sounders have been widely used in bathymetric surveys. Rather than a single line of points, multi-beam systems can map a wide swath beneath a ship's track (up to 10 times the water depth in deep water) (Kongsberg 2005). State-of-the-art acoustic swath-mapping systems can achieve 6 m spatial resolution and about 8 cm depth accuracy in 200 m water depth (Kongsberg 2005). However, ship-borne surveys are time consuming, costly, particularly in relatively shallow coastal waters where survey swaths are narrow. It may not be feasible to survey waters shallower than 2–3 m deep because of sound saturation or/and inaccessibility of survey vessels. In recent decades, airborne bathymetric LiDAR (Light Detection And Ranging) systems have been developed to map shallow coastal waters. While maximum penetration of LiDAR systems is heavily dependent upon water clarity, these systems commonly achieve depth measurements of up to 30 m, with 4 m spatial resolution and 20 cm vertical accuracy. The nominal maximum detectable depth is 40 m for SHOALS (Scanning Hydrographic Operational Airborne LiDAR Survey) developed by Optech Inc., Canada (Lillycrop and Banic 1993), 70 m for LADS (Laser Airborne Depth Sounder) developed by Tenix LADS Corporation, Australia (Stumpf et al. 2003; Finkl et al. 2005a), and 25 m for the NASA's EAARL (Experimental Advanced Airborne Research LiDAR) (Brock et al. 2004). While these airborne bathymetric LiDAR systems provide a rapid and precise means for mapping shallow coastal waters, their use is limited by the high cost of operations.

The feasibility of deriving bathymetric estimates from remote sensing imagery was first demonstrated using aerial photographs over clear shallow water (Lyzenga 1978). The technique has been expanded to include the use of passive optical multi-spectral satellite imagery including Landsat (Benny and Dawson 1983; Jupp et al. 1985; Lyzenga 1981; 1985), IKONOS (Stumpf et al. 2003), and QuickBird (Mishra et al. 2006; Conger et al. 2006) images. Historical archives of satellite images and aerial photographs are available worldwide. The temporal sequence of these images provides a way to document changes in seabed topography through time. Although optical remote sensing systems are limited by depth penetration and constrained by water turbidity, they provide a faster and lower-cost alternative to ship-borne bathymetric mapping in shallow water. These techniques are especially suitable for remote areas or hazardous coastal areas (e.g., with high surf) where ship operations are logistically problematic. The obvious advantages over conventional echo sounding methods include the wide data availability, synoptic surface coverage, and high spatial resolution. The only caveat is that remotely sensed images need to be carefully calibrated to ensure the accuracy of extracted depth information.

Several algorithms have been proposed and tested for bathymetric estimations in various environments by establishing the local relationship between image pixel values and known water depth values. Lyzenga (1978; 1981; 1985) proposed bathymetry algorithms for both a single wavelength band and a pair of wavelength bands. The single wavelength band algorithm is based on the assumption of invariant bottom type (reflectance) in the

scene. The algorithm for a pair of wavelength bands is a multiple log-linear regression model applicable to the scene in which the bottom type (reflectance) is variable. Benny and Dawson (1983) developed a bathymetry inversion algorithm by incorporating the solar elevation angle correction. Jupp (1989) proposed an algorithm that first calculates depth of penetration (DOP) zones for different bands and then calibrates depths within DOP zones. Philpot (1989) discussed the possible means to extend the inversion algorithm to more complex scenes where both bottom types (reflectance) and water quality (optical properties) vary spatially within the scene. Recently, Stumpf et al. (2003) proposed a novel non-linear inversion model that offers more accurate estimates for deeper benthic habitats and for shallow habitats with low reflectance (e.g., extremely dense algae or seagrass) compared to widely adopted log-linear inversion models. Legleiter et al. (2004) confirmed some of these advantages in the derivation of river channel depths from remote sensing data. Despite demonstrated advantages, the calibration of the non-linear inversion model is much more difficult than that of the conventional log-linear model whose parameters can be easily determined using the standard least-square regression approach. Stumpf et al. (2003) employed a trial-and-error method to fit manually the model parameters with a limited number of reference depth points. The manual calibration is laborious and time consuming, and cannot ensure optimal parameters for the inversion model.

This paper presents an automated method for calibrating the parameters for the non-linear inversion model proposed by Stumpf et al. (2003). Our method is based on the Levenberg-Marquardt optimization algorithm and is able to efficiently find optimal model parameters with an arbitrarily large set of reference depth points. We have implemented our calibration method using C++ programming language and successfully applied it to an IKONOS multispectral image over the south shore of Molokai Island, Hawaii. In the following sections, we will first review and summarize bathymetric inversion models and their underlying physical principles and then present the mathematical formation and implementation of our automated method for calibrating the non-linear bathymetric inversion model. Next, we examine and analyze our application results and then draw some final conclusions.

Bathymetric Inversion Models for Optical Multi-spectral Imagery

The fundamental physical principle underlying the retrieval of bathymetric information from optical remote sensing images is that when light passes through water it becomes attenuated by interaction with the water column. Deep areas appear dark on the image since the water absorbs much of the reflected light. Shallow areas appear lighter on the image since less light reflected from the seabed is absorbed in the passage through the water column.

The total upwelling radiance (L_t) recorded by the remote sensor consists of four components (Figure 1) (Jensen 2007): bottom radiance (L_b), subsurface volumetric radiance (L_v), specular radiance (L_s), and atmospheric path radiance (L_p) as shown in Eq. (1):

$$L_t = L_b + L_v + L_s + L_p \tag{1}$$

Atmospheric path radiance (L_p) is a function of atmospheric scattering, including both Rayleigh (molecular) scattering and Mie (aerosol) scattering. Subsurface volumetric radiance (L_v) results from volume scattering from the water and its organic/inorganic

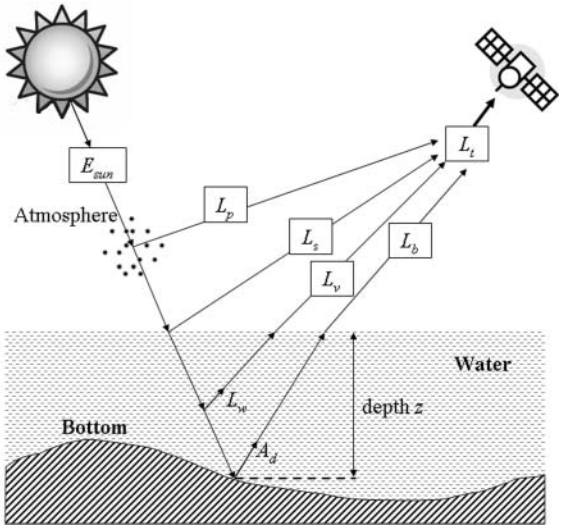

Figure 1. Four components of the total upwelling radiance measured by a remote sensor.

constituents (e.g. sediment and chlorophyll). It is closely related to the optical properties of the water column. Specular radiance (L_s) is the reflection from the water surface, including possible sunglint effects. The bottom radiance (L_b) is the energy reflected from the seabed, which integrates the information about water depth and bottom characteristics (habitat and substrate). To decode water depth information, we need to disaggregate bottom radiance (L_b) from total radiance (L_t). This is accomplished through atmospheric correction (Stumpf et al. 2003; Mishra et al. 2006) to remove L_p, sunglint correction (Lyzenga et al. 2006) to remove L_s, and deep water correction (Lyzenga 1978; 1985) to remove L_v. The measured total radiance over optically-deep water (L_∞) represents the combined effects of subsurface volumetric radiance, specular radiance, and atmospheric path radiance since the bottom radiance (L_b) equals zero for deep water. After atmospheric and sunglint corrections, the deep water radiance (L_∞) only contains subsurface volumetric radiance (L_v). Assuming that subsurface volumetric radiance in shallow water is the same as that of adjacent deep water, then optically deep water radiance (L_∞) recorded by the remote sensor can be used to correct the subsurface volumetric radiance (L_v) in shallow water. Based on Beer's Law, the intensity of light is attenuated exponentially with depth traveled through the water column, Lyzenga (1978; 1981; 1985) and Philpot (1989) proposed a simple radiative transfer model for optically shallow waters:

$$L = L_\infty[1 - \exp(-gz)] + A_d \exp(-gz) \tag{2}$$

where $L(= L_t - L_p - L_s)$ is the measured radiance after atmospheric and sunglint corrections, L_∞ is deep water radiance (equivalent to volumetric radiance L_v), A_d is the upwelling spectral radiance directly reflected from the bottom (before interacting with the overlying water column), g is a two-way attenuation coefficient, and z is depth. The second term on the left side of Eq. (2), $A_d \exp(-gz)$, accounts for the attenuation effect of passing through water of depth z, and equals the water leaving bottom radiance (L_b).

The bathymetric inversion model for a single spectral band can be derived from Eq. (2) as follows:

$$z = g^{-1}[\ln(A_d - L_\infty) - \ln(L - L_\infty)] \tag{3}$$

As shown in Eq. (3), the estimation of depth z from single band measurement L will depend on the determination of A_d and deep water radiance L_∞. Assuming that the ratio of bottom reflectance between two spectral bands is constant for all bottom types within a given scene, Lyzenga (1978; 1981; 1985) derived a bathymetric inversion model for two (and/or multiple) spectral bands as follows:

$$z = a_0 + \sum_{i=1}^{N} a_i \ln[L(\lambda_i) - L_\infty(\lambda_i)] \tag{4}$$

where a_i ($i = 0,1, \ldots, N$) are the constant coefficients, N is the number of spectral bands, $L(\lambda_i)$ is the remote sensing radiance after atmospheric and sunglint corrections for spectral band λ_i, and $L_\infty(\lambda_i)$ is the deepwater radiance for spectral band λ_i. The natural logarithm transformation produces a linear relationship between water depth and deepwater-corrected radiances of spectral bands. Eq. (4) is referred to as the log-linear inversion (or deepwater correction) model, which has been most widely used for estimating water depths from optical multi-spectral remote sensing imagery.

Recently, Stumpf et al. (2003) proposed a non-linear bathymetric inversion model based on a log-transformed band ratio:

$$z = m_1 \frac{\ln(nL(\lambda_2))}{\ln(nL(\lambda_1))} - m_0 \tag{5}$$

where m_0, m_1, and n are constant coefficients for the model, and $L(\lambda_1)$ and $L(\lambda_2)$are the remote sensing radiances (after atmospheric and sunglint corrections) for spectral bands λ_1 and λ_2. The basic premise of the above non-linear inversion model is that attenuation varies spectrally. Upwelling radiance in spectral bands with high attenuation will be less than that of bands with lower attenuation. Therefore, increasing depth will induce faster decreases in radiance for spectral bands with stronger attenuation. Substrate variability is accounted for implicitly through the ratio of logarithm-transformed radiances. A change in bottom albedo affects both bands similarly, while a change in depth has more pronounced effects on the band with greater attenuation. The ratio of the logarithm-transformed radiances will thus be more sensitive to depth than to bottom reflectance. The non-linear inversion model avoids the problem encountered for dark substrates such as dense macroalgae or sea grass. In those areas with dark substrate where radiance (L) is lower than deepwater radiance L_∞, depths cannot be derived from the log-linear inversion model as shown in Eq. (4). In addition, Stumpf et al. (2003) demonstrated that their non-linear inversion model is more robust and accurate than the conventional log-linear inversion model for relatively deep areas.

To minimize depth errors, wavelength bands with the smallest attenuation should be used both in the log-linear and non-linear bathymetric inversion models. Different wavelengths of light penetrate water to varying degrees. Blue light (440 to 540 nm) can penetrate clear down to 30 m depth, and thus serves as the optimum spectral band from which to extract depth information. Longer wavelengths attenuate rapidly in water. In clear waters, green light (500–600 nm) can penetrate to a maximum depth of approximately 15 m, red light (600–700 nm) to 5 m, and near infrared (700–800 nm) to 0.5 m (Green et al. 2000).

The depth of light penetration is also influenced by water turbidity. Suspended sediments, chlorophyll, and dissolved organic compounds increase turbidity and thus reduce the depth of light penetration.

Both the log-linear and non-linear bathymetric inversion models are based on the assumption that water optical properties (hence the attenuation coefficient and volumetric scattering) do not vary spatially within an image scene. This assumption would be met in areas with high and complete horizontal mixing, which leads to uniform water quality over a fairly large area. If the assumption is violated, however, and water quality does show significant spatial variation within the scene, depth estimates from the model will be subject to substantial errors. In addition, both models assume that the ratio of bottom reflectances in the two spectral bands is the same for different types of bottoms within a given scene. This assumption may be true for certain types of bottoms but not for all types. Therefore, both log-linear and non-linear inversion models can account for spatial heterogeneity in bottom type (substrate reflectance) to some extent. The ideal situation for depth retrieval from optical multispectral imagery occurs when water clarity is high, and both water quality and bottom type are uniform throughout the scene.

Calibration of Non-linear Inversion Model Based on Levenberg-Marquardt Method

To estimate absolute depths, all bathymetric inversion models must be calibrated using reference points where the true depths are known. The calibrated inversion model can then be applied to a multi-spectral image to compute depth at each pixel. The conventional log-linear inversion model for two spectral bands has three parameters (a_0, a_1, and a_2) requiring calibration. The model is calibrated empirically using the standard least-squares regression approach, which selects values for these parameters that minimize the difference between model-estimated depths and actual depths at a series of reference points. The non-linear inversion model proposed by Stumpf et al. (2003) also has three model parameters (m_0, m_1, and n). Due to its intrinsic non-linear form, however, the determination of optimal model parameters is more difficult. The use and further assessment of this non-linear inversion model has been hindered by the lack of an automated method for model calibration. Stumpf et al. (2003) tuned the model parameters manually with several reference points in a trial and error manner, but this method is only possible with a small number of reference depth points. The low number of reference points reduces the reliability of the calibration and the likelihood that optimal model parameters will be determined.

We have derived a numerical algorithm to automatically calibrate the parameters within the non-linear inversion model. The algorithm is based on the Levenberg-Marquardt optimization method (Press et al. 2002). Mathematically, the non-linear inversion model calibration problem is as follows: Given a set of observed depths, find the optimal model parameter values that minimize the differences between the estimated depths from the inversion model and the actual depths. A merit (error) function is defined to measure the agreement (difference) between model-estimated and observed depths. Using the least-squares fit method, the sum of the squares of the errors χ^2 is used as the merit function:

$$\chi^2(m_0, m_1, n) = \sum_{k=1}^{K} (\hat{Z}_k - Z_k)^2 = \sum_{k=1}^{K} \left[m_1 \frac{\ln(nL(\lambda_1)_k)}{\ln(nL(\lambda_2)_k)} - m_0 - Z_k \right]^2 \qquad (6)$$

where K is the number of points with a known depth, Z_k is the known (observed) depth

for point k, and $\hat{Z}_k$ is the estimated depth from the inversion model based on the spectral values at point k. Optimal values for the model parameters minimize the merit function χ^2.

The Levenberg-Marquardt method adopts an iterative procedure to yield the optimal (best-fit) model parameters. At each iteration step, the model parameters are adjusted and refined to reduce the value of the merit function. The Levenberg-Marquardt method is an elegant combination of the inverse Hessian matrix (the second derivative matrix) method and the steepest descent method (Press et al. 2002). The resulting fitting process rapidly converges to a reliable solution. When the parameter estimations are far from the minimum, the steepest descent method is used. As the minimum is approached, it smoothly switches to the inverse Hessian matrix method. We derived the first and second partial derivatives of the merit function $\chi^2(m_0, m_1, n)$ with respect to each of the three parameters for specifying the elements of the Hessian matrix in the minimization process. The automated iterative algorithm for calibrating the nonlinear bathymetric inversion model has been formulated as follows:

1. Given the known depth observation Z_k and initial estimates for the three parameters $m_0(0)$, $m_1(0)$, and $n(0)$, calculate $\chi^2(m_0(0), m_1(0), n(0))$ using Eq. (6);
2. Set λ to a modest value of 0.001;
3. Solve the simultaneous linear Eq. (7) for Δm_0, Δm_1, and Δn

$$\begin{cases} (1+\lambda)\frac{\partial^2\chi^2}{\partial m_0 \partial m_0}\Delta m_0 + \frac{\partial^2\chi^2}{\partial m_1 \partial m_0}\Delta m_1 + \frac{\partial^2\chi^2}{\partial n \partial m_0}\Delta n = -\frac{\partial\chi^2}{\partial m_0} \\ \frac{\partial^2\chi^2}{\partial m_0 \partial m_1}\Delta m_0 + (1+\lambda)\frac{\partial^2\chi^2}{\partial m_1 \partial m_1}\Delta m_1 + \frac{\partial^2\chi^2}{\partial n \partial m_1}\Delta n = -\frac{\partial\chi^2}{\partial m_1} \\ \frac{\partial^2\chi^2}{\partial m_0 \partial n}\Delta m_0 + \frac{\partial^2\chi^2}{\partial m_1 \partial n}\Delta m_1 + (1+\lambda)\frac{\partial^2\chi^2}{\partial n \partial n}\Delta n = -\frac{\partial\chi^2}{\partial n} \end{cases} \tag{7}$$

4. Evaluate $\chi^2(m_0(0) + \Delta m_0, m_1(0) + \Delta m_1, n(0) + \Delta n)$ using Eq. (6);
5. If $\chi^2(m_0(0) + \Delta m_0, m_1(0) + \Delta m_1, n(0) + \Delta n) \geq \chi^2(m_0(0), m_1(0), n(0))$, increase λ by a factor of 10 and go back to step 3); if $\chi^2(m_0(0) + \Delta m_0, m_1(0) + \Delta m_1, n(0) + \Delta n) < \chi^2(m_0(0), m_1(0), n(0))$, decrease λ by a factor of 10, and then update the initial estimates, namely, replace $m_0(0)$, $m_1(0)$, $n(0)$ by $m_0(0) + \Delta m_0$, $m_1(0) + \Delta m_1$, $n(0) + \Delta n$. Then go back to step 3) and perform the next round of iteration for refining the estimates for the three parameters.

The parameter λ controls the switching between the steepest descent method and the inverse Hessian matrix method. When λ is large, the steepest descent method is used. When λ approaches 0, the inverse Hessian matrix method is used. The convergence condition for stopping the iteration is that a change in the parameters only decreases the merit function $\chi^2(m_0, m_1, n)$ by a negligible amount specified by the user. After the convergence condition is satisfied, the final fitted parameters are computed by setting $\lambda = 0$ and inversing the matrix consisting of the coefficients on the left side of Eq. (7). The covariance matrix of the standard errors is also calculated at the final stage for analyzing the goodness-of-fit for each parameter.

We have implemented our calibration algorithm using C++ programming language and added it into ArcGIS environment as an extension tool. This tool will be freely available for public use. As demonstrated in the following section, our automated calibration algorithm is effective and efficient with a large number of reference depth points. Optimal parameters for the non-linear inversion model can be determined rapidly and reliably.

Application Results

Study Area and Data Sets

We performed a case study to evaluate the performance of our automated method for calibrating the non-linear bathymetric inversion model. The performance of the non-linear model is evaluated by comparison to the conventional log-linear inversion model. We performed the study using data from the central part of the south shore of Molokai Island, Hawaii (Figure 2). We used high resolution IKONOS satellite images for the remotely sensed imagery and Airborne marine LiDAR measurements from the SHOALS system for ground-truth depth points with which to calibrate and compare the performance of the two bathymetric inversion models.

Molokai Island is located in the north-central Pacific (roughly 21.15°N, 157.1°W) between the islands of Oahu and Maui in the Hawaiian archipelago (Figure 2). It has a moderate tropical climate with gentle northeasterly trade winds and mean annual rainfall of 689 mm. Average monthly temperature ranges from 21.2°C in February to 25.7°C in August. Our bathymetric analysis is conducted for a 16 km stretch of shallow waters along the south shore of Molokai. The substrates vary between sand, pavement, and live coral. Benthic biological cover includes various densities of algae and small corals. A major feature of the benthic habitats is the broad, shallow pavement platform of the reef flat, which extends nearly 1.5 km offshore. Sand patches and coral-covered pavement dominate the seaward edge of the reef flat. Offshore of the reef crest is the fore reef, which is characterized by shore-normal spur-and-groove structures and includes the zone of highest coral cover (Storlazzi et al. 2003; Cochran-Marquez 2005). The spatial heterogeneity in substrate reflectance and the diversity of benthic habitat types impose considerable challenges to depth retrieval from satellite multi-spectral imagery. In 2000, Airborne LiDAR data were collected along the south shore of Molokai by the SHOALS system of the US Army Corps of Engineers. The system operates from a deHavilland DHC-6 Twin Otter flying at 200–400 m altitude and a ground speed of about 100 knots. The depth points had horizontal accuracy of about 3 m, vertical accuracy of 15 cm, and a maximum depth of about 35 m. The depth measurements are referenced to the tidal datum MLLW (the Mean Lower Low Water). The precise depth measurements from the SHOALS are used in this research as ground-truth to calibrate and compare the performance of two bathymetry inversion models.

The two IKONOS multi-spectral image frames used in our analysis were acquired by the IKONOS-2 satellite on February 21, 2005. The color composition of the blue, green, and red bands of the two images is shown in Figure 2. At the image acquisition time (21:19 GMT), the sky was perfectly cloudless, and the sun had an elevation angle of 52.8 degrees, and azimuth angle of 145.07 degrees from the true north. The ocean waters off the island were calm and optically clear. The multi-spectral imagery has three visible bands (blue 450–520 nm, green 510–600 nm, red 630–700 nm) and one near infrared (NIR) band (760–850 nm) with a spatial resolution of 4 m. The IKONOS sensor has an instrument nominal sensitivity about fourfold greater than the Landsat-7 ETM+, and each band has 11-bit dynamic range per pixel.

The IKONOS images are Geo data products from Space Imaging, Inc. We employed PCI OrthoEngine software to perform the rigorous georeferencing and orthorectification (Toutin 2003). We collected 12 Ground Control Points (GCPs) for each image frame based on 1 m orthorectified aerial photographs and employed a 10 m Digital Elevation Model (DEM) for the orthorectification. The orthorectified aerial photographs and the DEM were created by Center for Coastal Monitoring and Assessment (CCMA) of National Oceanic and

Atmospheric Administration (NOAA) (http://www.soest.hawaii.edu/coasts/data/molokai/). With the GCPs and the DEM, we reconstructed the satellite orbital model and removed geometric and terrain distortions in the source IKONOS Geo data to create orthorectified images, using the UTM (zone 4N) projection and referenced to the WGS84 ellipsoid. By using independent check points, we evaluated the planimetric position accuracy of the orthorectified IKONOS images to be about 2.4 m (RMSE). Atmospheric corrections on the images have been performed using the ATCOR2 software package (Richter 1996). The ATCOR2 compiled atmospheric correction functions for different satellite sensors using the MODTRAN4 code (Berk et al. 1998) to perform radiative transfer calculations. The atmospheric correction functions are stored in ATCOR2 as look-up tables for different standard atmospheres (altitude profile of pressure and air temperature), different aerosol types and concentrations, and different ground elevations (Richter 1996). The aerosol type describes the absorption and scattering properties of the particles and determines the wavelength behavior of the path radiance. ATCOR2 supports four basic aerosol types: rural, urban, maritime, and desert. We selected the maritime tropical atmosphere option in ATCOR2 for the atmospheric correction. This option models the near sea surface aerosol and accounts for sea-salt particles produced by the evaporation of sea-spray droplets together with a background aerosol of pronounced continental character. This process produced atmospherically-corrected images in units of percent reflectance. The sun glint correction was performed using an approach outlined by Lyzenga et al. (2006). This approach relates the sun glint signal in visible bands to that in the near infrared band. Practically, the near infrared band does not contain volume scattering or bottom-reflected signal and the correction can be applied over the entire scene.

Model Calibrations

We used the blue and green bands of the IKONOS images and a set of reference depth points from the SHOALS to calibrate the bathymetric inversion models and derive a bathymetric grid for the entire scene. We randomly selected 2000 reference depth points surveyed by SHOALS system throughout the 16 km stretch of the south shore for model parameter calibration (Figure 3). First, a log-linear model was calibrated using the standard multiple regression approach. The log-linear model required the deep water correction. We selected a small area of optically-deep water and empirically determined the average reflectance values for the blue and green bands as their deep-water reflectances. The area of optically deep water consists of spatially connected pixels for which the reflectance values of all four bands are below the tenth-percentile reflectance magnitudes of corresponding bands for all pixels within the water area (Lyzenga et al. 2006). After subtracting the deep water reflectance from each band, we performed natural logarithm transformation of the difference values. The model parameters are optimally determined by regressing the selected reference depth points on the corresponding log-transformed (deepwater-corrected) reflectance values (Table 1).

Our automated calibration algorithm has been applied to the reference depth points to determine optimal parameters for the non-linear inversion model. The algorithm is efficient, and the convergence of the parameter fine-tuning process is achieved within six iterations with a total computation time of 15 seconds (Table 2). Our algorithm also provides the error and confidence interval estimates for the model parameters as shown in Table 3.

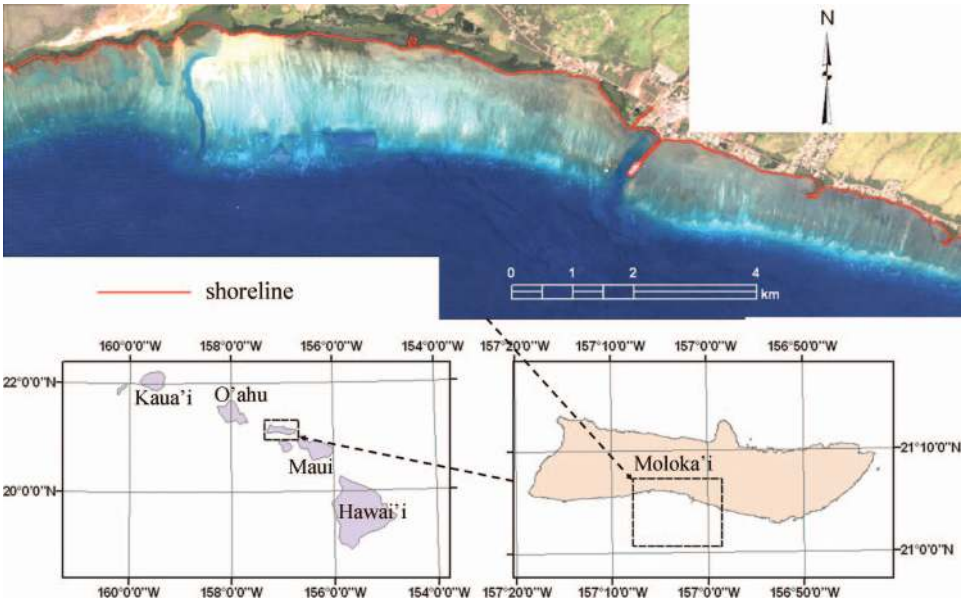

Figure 2. Location of Molokai Island and color composition of IKONOS blue, green, and red bands. (Please see online version of article for color version of this figure.)

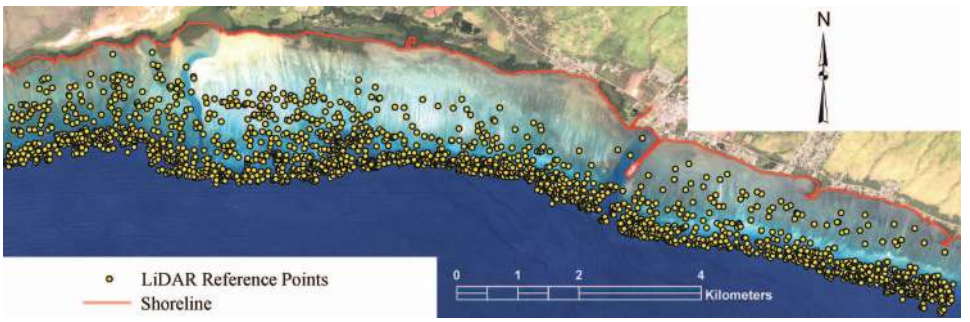

Figure 3. Spatial distribution of reference depth points used in model calibration. (Please see online version of article for color version of this figure.)

Table 1
Best-fit parameters for log-linear inversion model

Parameters	Best-fit	Std error	95% Confidence interval
a_0	11.140	0.328	[10.484, 11.796]
a_1	10.976	0.116	[10.744, 11.208]
a_2	−5.845	0.136	[−6.117, −5.573]

Table 2
Iterative fitting of optimal parameters for non-linear inversion model

Iteration	m_0	m_1	n	χ^2	$\frac{\Delta\chi^2}{\chi^2}$
0	41.073	35.006	111.172	11469.37	
1	39.993	34.009	103.611	11348.46	1.05%
2	31.433	25.527	70.830	11039.59	2.72%
3	21.640	15.888	51.894	10572.00	4.24%
4	23.266	17.503	56.087	10056.19	4.88%
5	23.497	17.734	57.025	10030.76	0.25%
6	23.467	17.706	56.991	10030.71	0.0005%

Performance Assessments

The performance of the non-linear inversion model is evaluated in comparison with the conventional log-linear model. To ensure the reliability of evaluation, we selected 1,496 independent check points from the SHOALS LiDAR measurements that were not used to calibrate model parameters. The model-predicted depths were plotted versus the ground truth depths for the independent check points (Figure 4). The scatter plot shows that both the log-linear and the non-linear inversion models produced acceptable depth estimates down to 20 m depth. The correlation coefficient between the model-estimated depths and the ground-truth depths is 0.935 for the log-linear inversion model and 0.932 for the non-linear inversion model. The Root Mean Squares Error (RMSE) was calculated for the different depth ranges and also for the entire set of check points. The magnitude of the prediction error increased with depth for both the log-linear and the non-linear inversion models as expected (Figure 4, Table 4). The non-linear inversion model offered slightly more accurate depth estimates for deeper (> 15 m) substrates than the log-linear inversion model, although their performances are very similar in terms of overall accuracy. The prediction residuals of both models are displayed in Figure 5 as histograms. The prediction error of the log-linear model has a normal distribution. The prediction error distribution of the non-linear model is skewed, indicating a slight overestimation tendency for the shallow areas (< 5 m).

We also calibrated both log-linear and non-linear inversion models to a greater depth range but found much greater error than we did for shallow waters. The RMSE for the 20–25 m depth range was larger than 4 m for both models. In contrast, the model accuracy increased considerably if the model parameters were calibrated for a shallower depth range. The RMSE of the non-linear inversion model can be reduced to 1.5 m if it is calibrated and applied in the 0–15 m depth range.

Table 3
Best-fit parameters for non-linear inversion model

Parameters	Best-fit	Std error	95% Confidence interval
m_0	17.706	0.258	[17.190, 18.222]
m_1	23.468	0.260	[22.948, 23.988]
n	56.991	0.503	[55.985, 57.997]

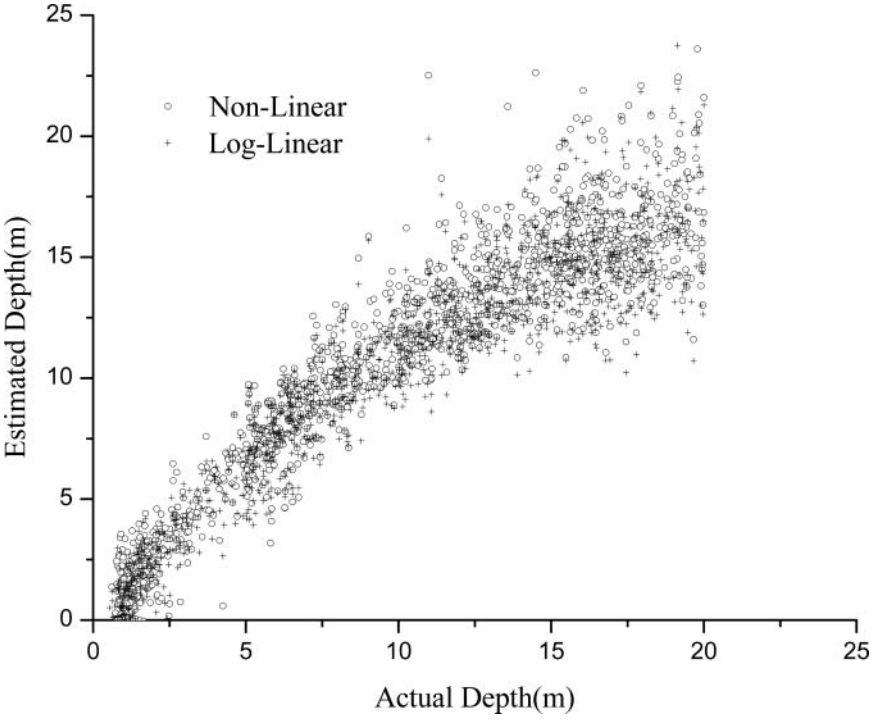

Figure 4. Scatter plots of estimated depths from log-linear and non-linear inversion models versus the ground truth depths.

After atmospheric correction, sun glint correction, and deep-water correction, the reflectance values of spectral bands are still a function of both water depth and substrate reflectance. Concerns remain whether a bathymetric inversion model can offer robust depth estimates in areas with spatially-varying bottom types. Although both the log-linear and non-linear inversion models can compensate for certain bottom type variations in theory, no previous empirical assessment of this theory has been reported. We investigate the robustness of the bathymetric inversion models to spatial variation in bottom types (substrate reflectance) by analyzing the spatial pattern of the model prediction residuals. If an inversion model is robust to bottom type variation, the prediction residual will be randomly distributed in space. Otherwise, we should be able to detect spatial clusters of positive or negative residuals. Figure 6 shows the spatial distribution of prediction residuals of 1,496 check points for both the log-linear and non-linear inversion models. Despite obvious differences in spatial patterns, positive and negative clusters can be detected

Table 4
Root mean squares errors of the estimated depths from log-linear and non-linear models

	0–5	5–10	10–15	15–20	Overall
Log-linear	1.34	2.01	1.65	3.00	2.10
Non-linear	2.07	2.17	1.63	2.87	2.20

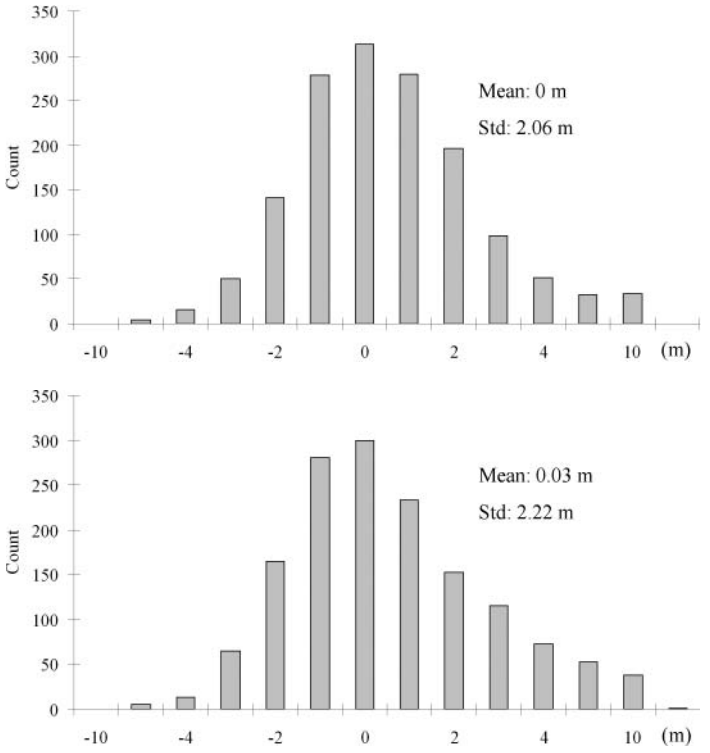

Figure 5. Frequency distribution of prediction residuals: (a) residual histogram of the log-linear inversion model; (b) residual histogram of the non-linear inversion model.

in the residual maps of both models. Therefore, it is certain that both log-linear and non-linear inversion models still suffer from the spatial heterogeneity in reflectance of various bottom types. As shown in Figure 6b, the non-linear inversion model systematically overestimates the depths in areas *A* and *C*, where the shallow pavement is covered by macroalgae, and systematically underestimates the depth in area *B*, where the pavement is uncolonized.

As shown in our assessment, the predicted-depth accuracy from IKONOS satellite images is about 1–2 m for shallow (0–15 m deep) substrates and about 3 m for deeper (15–20 m deep) substrates. This level of vertical accuracy is generally considered inadequate for navigational purposes in shallow waters. However, the derived bathymetric information is useful for many scientific and practical coastal management applications. The bathymetric grid derived from the non-linear inversion model at the spatial resolution of the IKONOS images (4 m) is shown in Figure 7. As shown in the hill-shaded relief images (Figure 7) and a three-dimensional perspective view of the seafloor (Figure 8), the high spatial resolution of the derived bathymetric data allow detection and recognition of various micro-morphological features such as sand grooves, coral spurs, blowouts, tidal channels, patch reefs, and aggregated reefs. The rugosity of the seabed increases from near shore to the reef base (Figures 7 and 8). The pavements on the reef flat are smooth and relatively feature-less. The morphology of the fore reef is dominated by typical spur-and-groove formations.

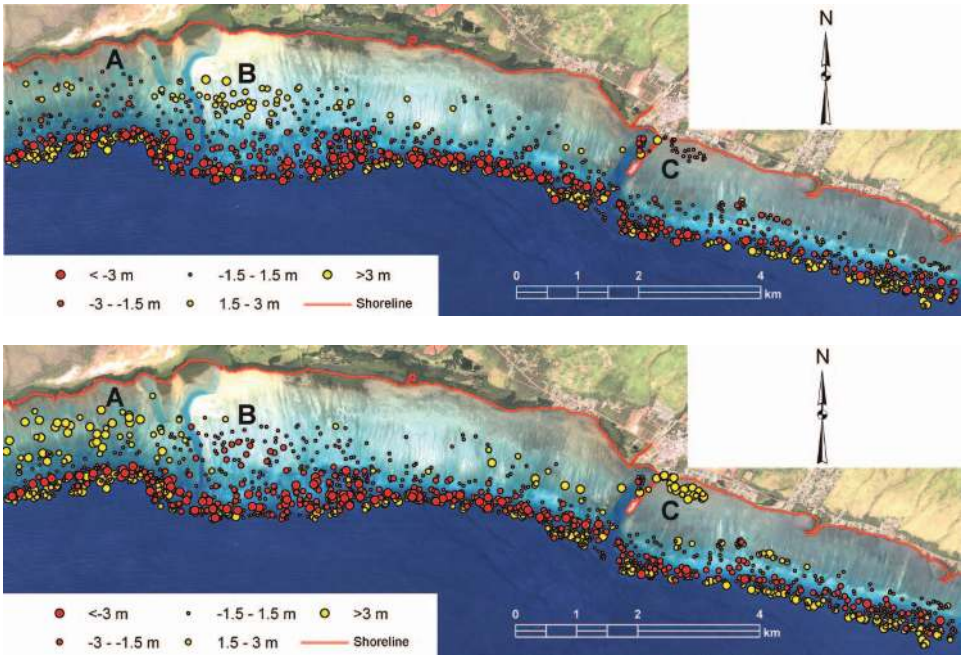

Figure 6. Spatial distribution and pattern of prediction residuals: (a) from the log-linear inversion model; (b) from non-linear inversion model. (Please see online version of article for color version of this figure.)

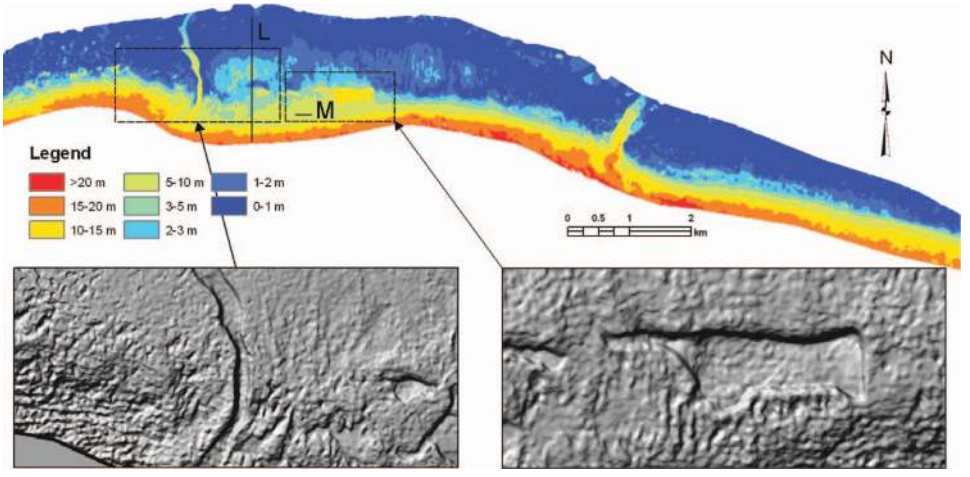

Figure 7. Bathymetric grid derived from IKONOS image using the non-linear inversion model. (Please see online version of article for color version of this figure.)

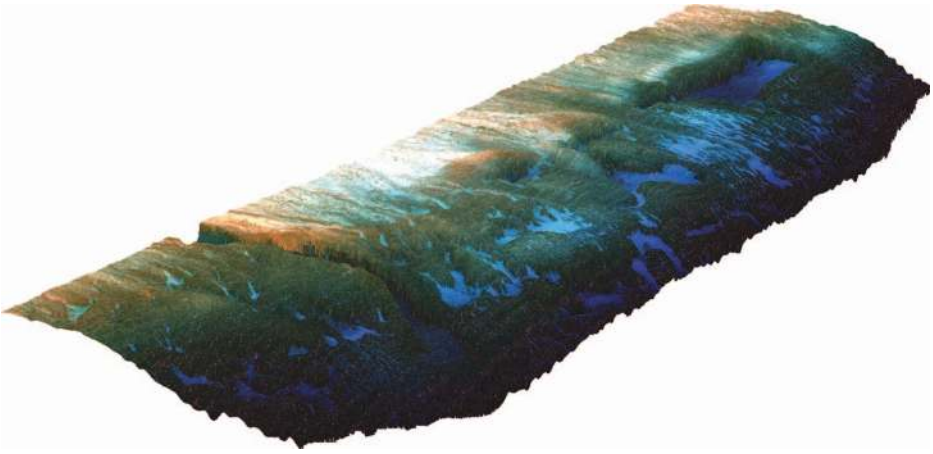

Figure 8. Three-dimensional perspective view of the reef morphology created by draping IKONOS image on top of the bathymetric grid from the non-linear inversion model. (Please see online version of article for color version of this figure.)

Quantitative descriptions of reef morphology can be conducted using shore-normal and shore-parallel depth profiles. Figure 9a shows a shore-normal depth profile along transect *L* marked in Figure 7. This profile clearly indicates the spatial extent and positions of the reef flat, reef crest, and fore reef. Figure 9b is a shore-parallel profile that cuts across the spur-and-groove structures along transect *M* in Figure 7. The bathymetric variation in this profile can be interpreted to estimate the spur height (0.7 m), width (50–70 m), and distance (wavelength) between adjacent spur crests (about 100 m). Clearly, bathymetric information derived from satellite multispectral imagery is valuable for extracting and quantifying fine-scale morphological features on shallow ocean floors.

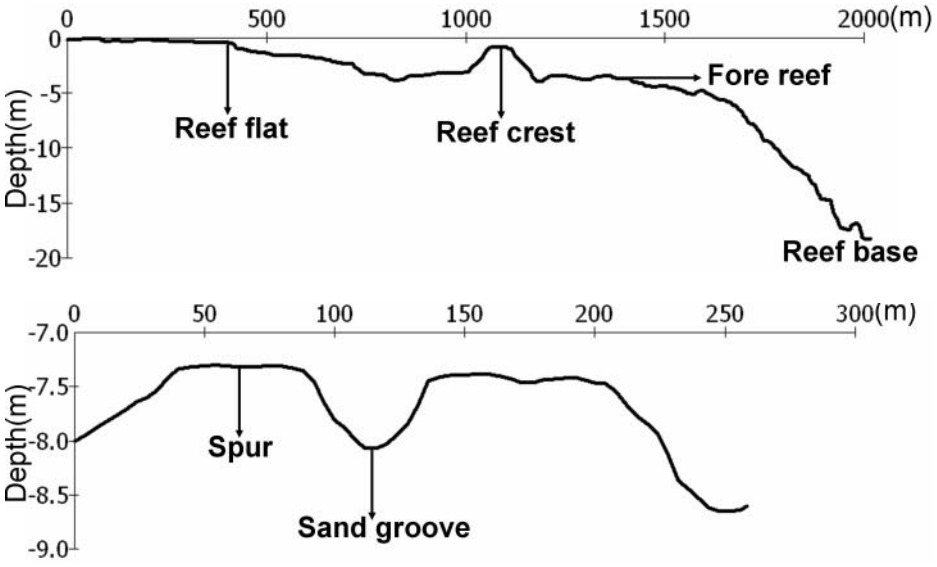

Figure 9. Bathymetric profiles: (a) shore-normal profile along transect *L*; (b) shore-parallel profile along transect *M*. Locations of transects *L* and *M* are marked in Figure 7.

Conclusions

An increasing number of studies have shown that bathymetric information can be derived from optical satellite multispectral imagery at the spatial resolution of the source image. Various inversion models have been developed to convert image pixel values into depth estimates. The log-linear inversion model developed by Lyzenga (1978) is the most popular among them. Recently, a non-linear inversion model has been proposed by Stumpf et al. (2003), who has demonstrated some desirable properties of this model. However, the lack of an automated calibration method has limited its use and further evaluation. By using the Levenberg-Marquardt optimization approach, we have derived and implemented an algorithm for automatic calibration of the non-linear inversion model with an arbitrarily large set of reference points. Our application example suggests that our calibration algorithm is efficient and reliable for identifying optimal parameters for the non-linear inversion model.

Our comparisons suggest that the overall performance of the non-linear inversion model is similar to that of the conventional log-linear inversion model. The non-linear inversion model can produce slightly more accurate depth estimates for areas deeper than 10–15 m but slightly less accurate for very shallow areas (<5 m). It is still uncertain whether or not the non-linear inversion model is superior to the conventional log-linear model. Further extensive assessments with various benthic environments are needed in order to make a firm conclusion.

Our case study of Molokai illustrated that depth estimates can be derived from high-resolution IKONOS multi-spectral imagery with vertical accuracy of about 2 m (RMSE) in water depths down to 20 m. Although this level of vertical accuracy does not meet International Hydrographic Office (IHO) standards for safe navigation, these bathymetric data are highly valuable for many other purposes. Bathymetric information retrieval from optical satellite multispectral imagery enjoys the advantages of large surface coverage, high spatial resolution, and low-cost. As demonstrated, subtle and detailed morphological features can be detected and quantified using the image-derived bathymetric data. Given that expansive areas of coastal bathymetry are still unsurveyed, bathymetric data derived from optical multispectral remote sensing imagery represents a valuable alternative to costly ship-borne echo sounding and airborne LiDAR surveys. This is particularly true for remote areas and developing countries.

To gain insight into model performance over variable bottoms types, we compared the spatial pattern of prediction from residuals for both log-linear and non-linear inversion models. Although in theory, both models account for spatial variations in bottom reflectance, our analysis suggests that much of the model estimate error is caused by spatial heterogeneity in substrate reflectance. Depth estimates were significantly overestimated or underestimated for several bottom types using both log-linear and non-linear inversion models. Apparently, further research is required to improve existing inversion models or to develop new, more robust inversion models for handling variable bottom types in the future.

Acknowledgements

This research is funded by the NOAA Sea Grant Program #NA16RG1078 and Norman Hackerman Advanced Research Program 010366-0017-2007.

References

Benny, A. H., and G. J. Dawson. 1983. Satellite imagery as an aid to bathymetric charting in the Red Sea. *The Cartographic Journal* 20:5–16.

Berk, A., L. S. Bernstein, G. P. Anderson, P. K. Acharya, D. C. Robertson, J. H. Chetwynd, and S. M. Adler-Golden. 1998. MODTRAN cloud and multiple scattering upgrades with application to AVIRIS. *Remote Sensing of Environment* 65:367–375.

Brock, J. C., C. W. Wright, T. D. Clayton, and A. Nayegandhi. 2004. LIDAR optical rugosity of coral reefs in Biscayne National Park, Florida. *Coral Reefs* 23:48–59.

Cochran-Marquez, S. A. 2005. Moloka'i benthic habitat mapping. In U.S. geological survey open file report, 18.

Conger, C. L., E. J. Hochberg, C. H. Fletcher, and M. J. Atkinson. 2006. Decorrelating remote sensing color bands from bathymetry in optically shallow waters. *IEEE transactions on Geoscience and Remote Sensing* 44:1655–1660.

Finkl, C. W., L. Benedet, and J. L. Andrews. 2005a. Interpretation of seabed geomorphology based on spatial analysis of high-density airborne laser bathymetry. *Journal of Coastal Research* 21:501–514.

Finkl, C. W., L. Benedet, and J. L. Andrews. 2005b. Submarine geomorphology of the continental shelf off Southeast Florida based on interpretation of airborne laser bathymetry. *Journal of Coastal Research* 21:1178–1190.

Green, E. P., P. J. Mumby, A. J. Edwards, and C. D. Clark. 2000. Remote sensing handbook for tropical coastal management. Paris: A. J. Edwards, UNESCO.

Jensen, J. R. 2007. Remote sensing of the environment: An earth resource perspective, 2nd ed. Upper Saddle River, NJ: Prentice Hall.

Jupp, D. L. B., K. K. Mayo, D. A. Kuchler, D. V. R. Claasen, R. A. Kenchington, and P. R. Guerin. 1985. Remote sensing for planning and managing the great Barrier Reef of Australia. *Photogrammetria* 40:21–42.

Jupp, D. L. B. 1989. Background and extension to depth of penetration(DOP) mapping in shallow coastal waters. Conference on Remote Sensing Application Projects Using microBRIAN Image Processing System.

Kongsberg. 2005. EM120 multibeam echo sounder. Retrieved Aug. 5, 2008, from http://www.knogsberg.com

Legleiter, C. J., D. A. Roberts, W. A. Marcus, and M. A. Fonstad. 2004. Passive optical remote sensing of river channel morphology and in-stream habitat: Physical basis and feasibility. *Remote Sensing of Environment* 93:493–510.

Lillycrop, W. J., and J. R. Banic. 1993. Advancements in the U.S. Army Corps of Engineers hydrographic survey capabilities: The SHOALS system. *Marine Geodesy* 15:177–185.

Lyzenga, D. R. 1978. Passive remote sensing techniques for mapping water depth and bottom features. *Applied Optics* 17:379–383.

Lyzenga, D. R. 1981. Remote sensing of bottom reflectance and water attenuation parameters in shallow water using aircraft and Landsat data. *International Journal of Remote Sensing* 2:71–82.

Lyzenga, D. R. 1985. Shallow-water bathymetry using combined lidar and passive multispectral scanner data. *International Journal of Remote Sensing* 6:115–125.

Lyzenga, D. R., N. P. Malinas, and F. J. Tanis. 2006. Multispectral bathymetry using a simple physically based algorithm. *Geoscience and Remote Sensing, IEEE Transactions on* 44:2251–2259.

Mishra, D., S. Narumalani, D. Rundqulst, and M. Lawson. 2006. Benthic habitat mapping in tropical marine environments using QuickBird multispectral data. *Photogrammetric Engineering & Remote Sensing* 72:1037–1048.

Mumby, P. J., C. D. Clark, E. P. Green, and A. J. Edwards. 1998. Benefits of water column correction and contextual editing for mapping coral reefs. *International Journal of Remote Sensing* 19:203–210.

Philpot, W. 1989. Bathymetric mapping with passive multispectral imagery. *Applied Optics* 28:1569–1578.

Press, W. H., S. A. Teukolsky, W. T. Vetterling, and B. P. Flannery. 2002. Numerical recipes, 2nd ed. New York: Cambridge University Press.

Richter, R. 1996. A spatially adaptive fast atmospheric correction algorithm. *International Journal of Remote Sensing* 17:1201–1214.

Smith, W. H. F., and D. T. Sandwell. 1997. Global sea floor topography from satellite altimetry and ship depth soundings. *Science* 277:1956–1962.

Storlazzi, C. D., J. B. Logan, and M. E. Field. 2003. Quantitative morphology of a fringing reef tract from high-resolution laser bathymetry: Southern Molokai, Hawaii. *Bulletin of the Geological Society of America* 115:1344–1355.

Stumpf, R. P., K. Holderied, and M. Sinclair. 2003. Determination of water depth with high-resolution satellite imagery over variable bottom types. *Limnology and Oceanography* 48:547–556.

Toutin, T. 2003. Error tracking in Ikonos geometric processing using a 3D parametric model. *Photogrammetric Engineering & Remote Sensing* 69:43–51.